Performance of nanocrystalline Ni_3N as a negative electrode for sodium-ion batteries

Xianji Li, Mahboba M. Hasan, Andrew L. Hector and John R. Owen

Chemistry, University of Southampton, Highfield, Southampton SO17 1BJ, UK

A.L.Hector@soton.ac.uk

Abstract

Nickel nitride is synthesised by high temperature ammonolysis of nickel(II) hexamine and *tris*(ethylenediamine) salts. Its electrochemical characteristics are examined in half cells vs lithium and sodium. Samples with high surface area are found to have significant reversible charge storage capacity in sodium cells and hence to be a promising negative electrode material for sodium-ion batteries.

Introduction

Battery technology has been fundamental to the development of portable electronics over recent years, and the development of green energy technologies and electric vehicles are powerful drivers for further improvement. Lithium-ion batteries provide high energy density and are currently the leading technology to address these energy storage requirements.[1] However, due to the limited reserves and the increasing price of exploitable lithium raw materials[2], there is a need for alternative competitive battery technologies. Sodium based energy storage devices could provide a high voltage and energy density similar to that achieved with lithium-ion batteries[2] and the abundance and low cost of sodium are a distinct advantage, especially for larger scale devices such as those needed for electric vehicles.

Taking inspiration from lithium-ion batteries,[3] most reports on sodium-ion batteries have used metal intercalating materials in the positive electrodes such as layered transition metal oxide[4, 5] and olivine[6] materials. A number of recent reports show good performance in positive electrode materials for sodium-ion batteries.[7-11] Cao *et al* reported a capacity of 128 $mAhg^{-1}$ in $Na_4Mn_9O_{18}$ nanowires at a charge/discharge rate of 0.1C (0.1 × theoretical capacity per hour) and 77% capacity retention after 1000 cycles at a rate of 0.5 C.[8] Tepavcevic *et al* obtained around 250 mAh/g capacity at a cycling rate of 0.08C from nanostructured bilayered V_2O_5.[10] Goodenough and co-workers recently reported a prussian blue framework structure with a reversible capacity of around 100 mAh g^{-1} and no capacity fade in 30 cycles.[11]

Graphite is widely employed as the negative electrode material for lithium-ion batteries as it can intercalate large amounts of lithium (up to one per C_6 unit) and retains a low potential even with small lithium loadings. It does not intercalate sodium and so cannot be used for sodium-ion batteries,[12] hence the negative electrode is a key challenge for the development of viable sodium ion batteries. Carbon-based materials still dominate the negative electrode literature for sodium-ion batteries.[2, 13-16] The first successful use of a carbon material, from decomposition of a glucose precursor, was published by Stevens *et al.*[13] Alcántara *et al* reported that carbon black can offer a first cycle reversible capacity close to 200 $mAhg^{-1}$ at very low oxidation/reduction rates (0.0125C).[14] More recently, Wenzel *et al* used porous silica templates to prepare templated carbon which can provide a 180 $mAhg^{-1}$ capacity in the first reduction cycle at 0.5C, which decreased to around 120 $mAhg^{-1}$ after 40 cycles.[15] This is still a good cycling performance compared with most published carbon materials. Very recently Cao *et al* reported hollow carbon nanowires prepared from pyrolysis of hollow polyaniline nanowires that can deliver an initial capacity of 251 $mAhg^{-1}$ and retain 206.3 $mAhg^{-1}$ after 400 cycles at 0.2C, a better cyclability than any other carbon-based material.[16] A non- carbon-based material, NASICON-type $NaTi_2(PO_4)_3$ was reported by Park *et al*[17] to provide around 120 $mAhg^{-1}$ capacity over 30 cycles, at a sodium insertion potential of 2.1 V versus Na/Na^+. A number of authors have also very recently shown good cycling performance in Sn, Sb and SnSb alloy materials.[18-21]

In recent years, conversion reaction mechanisms have been intensively investigated for lithium-ion batteries,[22] and transition metal nitrides are one promising group of materials[23-26] operating via the general reaction:

$$M_aN_b + 3bLi^+ + 3be^- \rightarrow aM + bLi_3N$$

The forward (reduction) process in this reaction would occur during charging if the material were in use as a negative electrode, or during discharge (at higher potential) during use as a positive electrode. Nickel nitride (Ni_3N) has been examined as a negative electrode material via conversion reactions for lithium-ion batteries, and the conversion mechanism in these electrodes was demonstrated by the presence of nickel metal observed by ex-situ diffraction measurements on thin film electrodes.[24] Despite an already high theoretical capacity of 423 $mAhg^{-1}$ based on the above reaction, nanosized Ni_3N prepared from decomposition of nickel amide achieved a specific capacity of 1200 $mAhg^{-1}$ in the first reduction reaction.[27] This capacity is not recovered on oxidation and quickly diminished on subsequent cycling, hence

the performance of Ni_3N is not competitive with other materials. However, negative electrodes for sodium-ion applications are less well developed and performance in a sodium-ion environment at the level exhibited by Ni_3N under lithium-ion conditions would be of interest. This paper describes the behaviour of nanocrystalline Ni_3N in a sodium-ion battery environment.

Experimental

Nickel nitride was synthesized in two ways:

1) Nickel (II) nitrate hexahydrate (4 g) was dissolved in deionised water (5 cm^3) and 35% ammonia solution (10 cm^3, Fisher) was added slowly with stirring to produce a bluish-violet solution. This solution was dried by evaporation under flowing ammonia and further dried in a dessicator over BaO for three weeks. After grinding the precursor was heated at 335 °C for 6 h followed by 200 °C for 8 h under flowing ammonia (BOC anhydrous grade, further dried by flowing over 3 Å molecular sieves).

2) Nickel(II) nitrate hexahydrate (1 g, Aldrich) was dissolved in ethanol (10 cm^3) with stirring and dried by removing the solvent *in vacuo* with gentle warming. The resulting yellow solid was dissolved in ethanol (5 cm^3) and ethylenediamine (2 cm^3, Aldrich, 99%) was added drop wise. Pink nickel *tris*(ethylenediamine) nitrate was recovered by removing solvent *in vacuo*. This solid was heated at 360 °C for 4 h then 200 °C for 40 h under flowing ammonia.

Powder X-ray diffraction (PXD) patterns were recorded on a Siemens D5000 diffractometer using monochromatic Cu-$K_{\alpha 1}$ radiation. Thermogravimetric analyses (TGA) used a Mettler-Toledo TGA/SDTA85le with flowing argon (50 ml/min). The temperature was raised from 25 to 800 °C at 10 °C/min and was held at maximum temperature for 20 or 60 minutes. The morphology was examined by transmission electron microscopy (TEM) on a Hitachi H7000 with an accelerating voltage of 75 kV, using samples prepared by ultrasound dispersion into distilled methanol and dropping onto carbon grids. Infrared (IR) spectra were recorded on a Perkin Elmer Spectrum 100 FTIR with samples prepared as KBr discs. Surface areas were calculated using the Brunauer-Emmett-Teller (BET) method[28] with nitrogen adsorption data collected using a Gemini 2375 Surface Area Analyser. Samples were sent for combustion microanalysis (C, H and N) to Medac Ltd.

Electrochemical cells were assembled in two-electrode Swagelok cells using sodium metal foil (Aldrich, 99.9%) as the counter electrode. Two sheets of Whatman GF/D borosilicate glass fibre were used as separator, soaked with 1 M $NaPF_6$ in ethylene carbonate/diethyl carbonate (1:1) electrolyte. The electrolyte components were separately dried (solvents dried by distillation from BaO and $NaPF_6$ dried under vacuum at 120 °C) before combining in the glove box. Electrochemical testing used a Bio-Logic SP150 potentiostat. The working electrode consisted of a powdered mixture of 75% active material with 20% of acetylene black (Shawinigan, Chevron Phillips Chemical Co. LP) and 5% PTFE rolled into a 90 μm thick sheet and then cut into a 10 mm diameter disc.

Results and discussion

The synthesis of Ni_3N from reaction of a nickel hexamine salt with ammonia was previously described by Gajbhiye *et al*.[29] We found that $[Ni(NH_3)_6].2NO_3$ tended to lose ammonia on drying and that good samples, that converted effectively to Ni_3N without NiO contamination, could only be obtained by drying in a dessicator flushed with gaseous ammonia (over a BaO drying agent). Most samples contained a small amount of nickel metal in the product and the amount of this impurity increased with synthesis temperature, but carrying out reactions at 335 °C then reducing the temperature to 200 °C for 8 hours resulted in a phase pure material by PXD. Rietveld refinement of the diffraction data (Fig. 1) yielded lattice parameters of a=4.62231(14) and c=4.30630(13) Å, which are close to the reported values of a=4.624(4) and c=4.316(4) Å.[29] Crystallite size was determined from the Lorentzian components of the profile fit[30] to be around 50 nm which is similar to the overall particle size observed in TEM images (Fig. 1). These images also show that the nano-sized particles are quite aggregated.

Thermogravimetric analysis (TGA) shows that the sample obtained from nickel hexamine nitrate loses approximately 7.8% of its mass in a single sharp mass loss just above 400 °C. Ni_3N contains 7.4% N and hence this mass loss is consistent with decomposition to nickel metal and nitrogen. Elemental analysis of this material showed it contained 7.3% N, 0.1% C and undetectable amounts of H (<0.1%). Nitrogen adsorption (BET) measurements showed these samples to have a fairly small surface area of 2.8 m^2g^{-1}, consistent with the relatively large and aggregated crystallites.

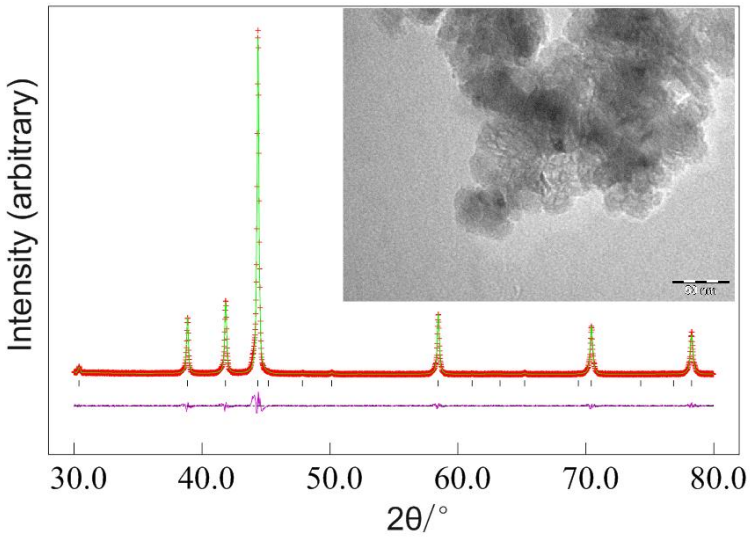

Fig. 1 Rietveld fit (R_{wp} = 13.0%, R_p = 9.1%) to the PXD data for Ni_3N produced from ammonolysis of $[Ni(NH_3)_6].2NO_3$. Crosses mark the data points, the upper continuous line the fit and the lower continuous line the difference. Tick marks show the allowed positions of reflections for Ni_3N with space group $P6_322$. Inset TEM image (scale bar = 50 nm) of Ni_3N produced by this route.

Electrochemical charge storage often benefits from smaller particle sizes, which reduce the length of the ion diffusion pathways that need to operate in the particles during charge and discharge. In order to obtain Ni_3N with a smaller particle size, nickel trisethylenediamine nitrate was also prepared and subjected to ammonolysis reactions. The optimal temperature for these reactions was 360 °C, higher than for Ni_3N synthesis from $[Ni(NH_3)_6].2NO_3$. These samples always contained a small quantity of nickel metal and this could not be converted to Ni_3N by applying a lower temperature step. Fig. 2 shows broader peaks in the diffraction pattern than those observed in Fig. 1. The refined Ni_3N lattice parameters varied slightly more from literature values, with a=4.5937(4) and c=4.3258(7) Å, and the crystallite size is around 11 nm. TEM images showed aggregated particles of approximately 20 nm size, with the deviation from that observed by diffraction suggesting the presence of some further disorder in the crystal structure of these particles.

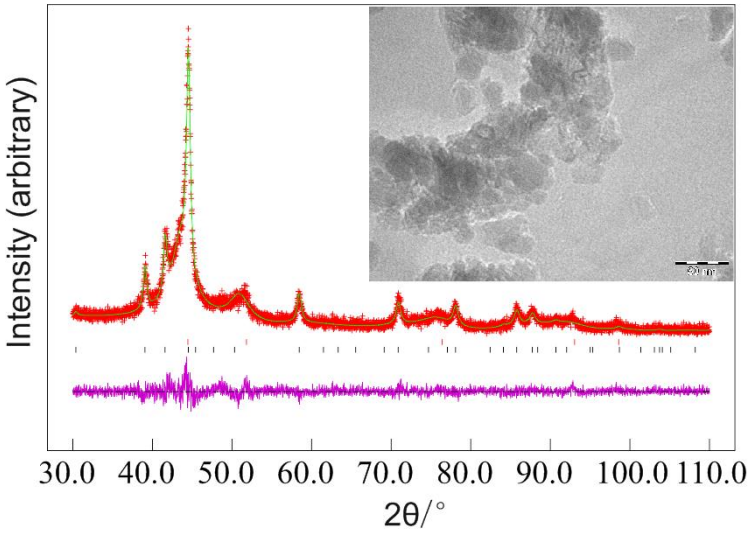

Fig. 2 Rietveld fit (R_{wp} = 13.5%, R_p = 10.3%) to the PXD data for Ni_3N produced from ammonolysis of $[Ni(EDA)_3].2NO_3$. Crosses mark the data points, the upper continuous line the fit and the lower continuous line the difference. The lower tick marks show the allowed positions of reflections for Ni_3N with space group $P6_322$, and the upper tick marks those of Ni metal. Inset TEM image (scale bar = 50 nm) of Ni_3N produced by this route.

TGA shows a much larger mass loss of ~20% from these samples over a broader temperature range than that observed with the nickel hexamine-derived samples, Fig. 3. Previous studies into the formation of metal nitrides from imide-amide polymers have shown that these systems lose most amide and alkylamide groups in this temperature range.[26] Elemental analysis shows the samples to contain 18.2% C, 1.7% H and 16.5% N and hence these samples are not phase pure Ni_3N. The IR spectra show amine groups in the form of absorptions at 3150 cm^{-1} (ν(NH)) and 1599 cm^{-1} (δ(NH_2)), and organic material through the shoulder on the low energy side of the ν(NH) peak.[31, 32] Overall, this material can be considered to consist of nanoparticulate, crystalline Ni_3N with a significant surface coating of organic materials. Nitrogen adsorption (BET) measurements showed a higher surface area in this material of 16.0 $m^2 g^{-1}$ compared with the more crystalline sample.

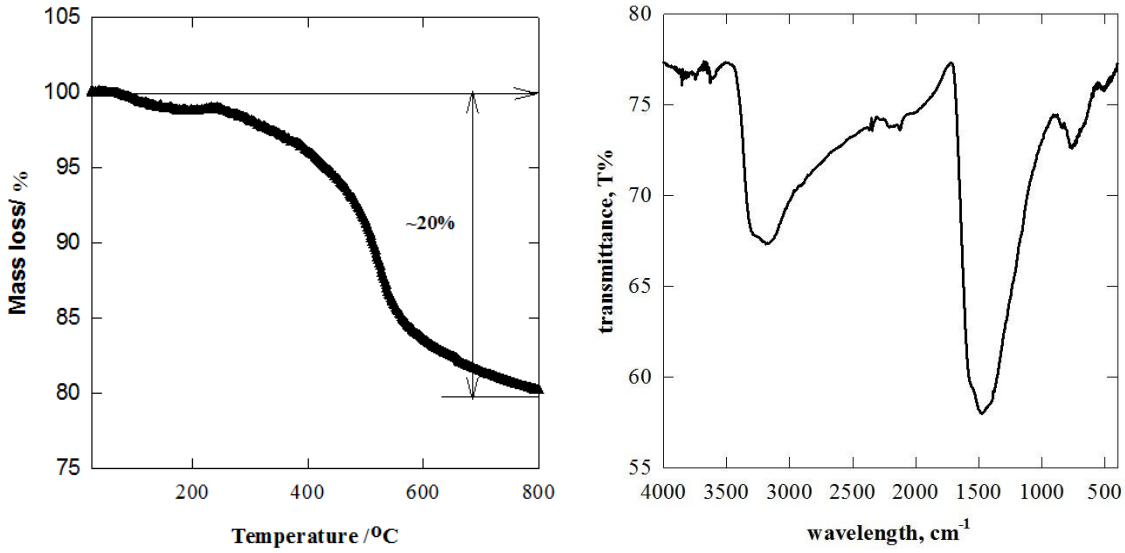

Fig. 3 TGA trace (left) and IR spectrum (right) of Ni_3N derived from ammonolysis of $[Ni(EDA)_3].2NO_3$.

Galvanostatic cycling of the $[Ni(EDA)_3].2NO_3$-derived Ni_3N samples vs Li showed very similar results to those recently reported by Gillot *et al* using nickel amide-derived Ni_3N.[22] During the first reduction at 1C (a rate determined such that theoretical capacity of 423 $mAhg^{-1}$ would be achieved in 1 h), 840 $mAhg^{-1}$ of charge was passed as the potential fell from 3 V to 1 mV. However, much of this is believed to be irreversible capacity due to solid-electrolyte interface (SEI)-forming side reactions and the reversible capacity is better evaluated for the subsequent oxidation cycles over the same potential range. The oxidation specific capacity for the first oxidation was about 400 $mAhg^{-1}$ and this value fell smoothly to ~210 $mAhg^{-1}$ after 30 cycles. At a faster rate of 5C (2115 mAg^{-1}) the capacities were lower (230 $mAhg^{-1}$ in the first reduction and 120 $mAhg^{-1}$ in the first oxidation) but the capacity profile was more level on cycling, delivering 108 $mAhg^{-1}$ in the 3rd oxidation and 98 $mAhg^{-1}$ in the 30th oxidation. These data are presented more fully in the supplementary information (Fig. S1).

Ni_3N samples were tested for their reduction-oxidation behaviour vs sodium foil using 1M $NaPF_6$ in EC:DEC (1:1) as the electrolyte.[33] Initially the behaviours of the two types of Ni_3N prepared in this study were compared with reduction/oxidation rates of 0.5C (211 mAg^{-1}). Most of the oxidation profile is observed below 1.5 V and hence use of Ni_3N as a negative electrode in high voltage cells, where the oxidation process would occur during cell discharge, is feasible. The first reduction cycle showed a capacity of 120 $mAhg^{-1}$ in the $[Ni(NH_3)_6].2NO_3$-derived Ni_3N and 465 $mAhg^{-1}$ in the $[Ni(EDA)_3].2NO_3$-derived material

(Fig. 4). In both cases the capacity fell significantly in the first 5 cycles, presumably due to SEI formation as observed in Li cells, but then stabilised and maintained fairly constant values after 30 cycles. In the higher surface area $[Ni(EDA)_3].2NO_3$-derived sample the 30th reduction cycle showed a specific capacity of 126 mAhg^{-1}. The higher capacity from the $[Ni(EDA)_3].2NO_3$-derived material shows that despite the expected conversion mechanism the particle size is still very significant in determining the capacity that can be derived from Ni_3N. Hence further cycling studies focussed on this smaller particle size material.

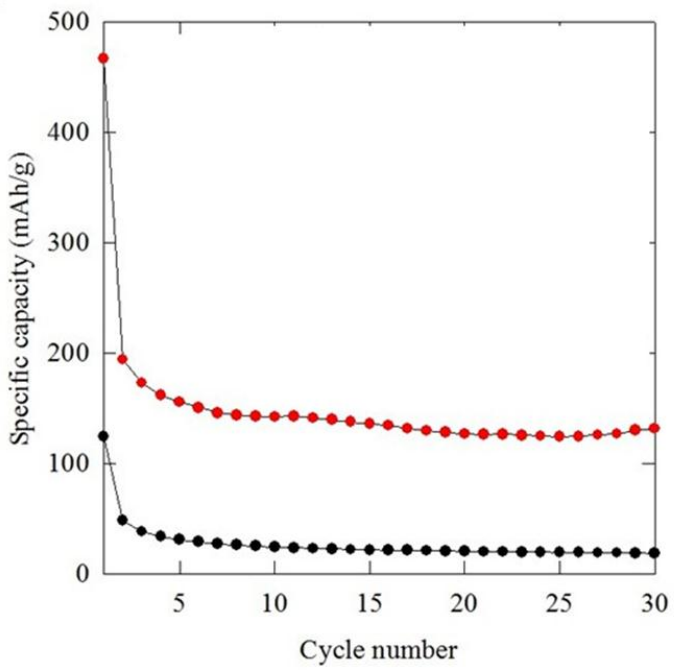

Fig. 4 Reduction specific capacity vs cycle number of Ni_3N-sodium half cells using $[Ni(EDA)_3].2NO_3$-derived Ni_3N (top) and $[Ni(NH_3)_6].2NO_3$-derived Ni_3N (bottom) cycled between 1 mV and 3 V at 0.5C (211 mAg^{-1}) for 30 cycles.

The loss of current to SEI formation during initial cycles means that consideration of the oxidation process, which is discharge in the context of using Ni_3N as the negative electrode in a sodium-ion cell, and the Coulombic efficiency (charge passed on discharging/oxidation divided by charge passed on charging/reduction) is as important as the specific capacity. Fig. 5 shows this data for $[Ni(EDA)_3].2NO_3$-derived Ni_3N-sodium half cells cycling at various current rates. It is striking that at all three rates the reduction and oxidation curves are close together, and hence the Coulombic efficiency is close to 100%, from the third cycle. This suggests that irreversible processes such as SEI formation are close to complete at this point. The specific capacity is always greater at lower reduction/oxidation rates, e.g. the first reduction process requires 517 mAhg^{-1} of charge at 0.1C (42.3 mAg^{-1}) but only 326 mAhg^{-1}

at 1C (423 mAg^{-1}). The first oxidation delivers 137 (1C), 193 (0.5C) or 227 (0.1C) $mAhg^{-1}$ and after 20 cycles these values fall to 80 (1C), 126 (0.5C) or 134 (0.1C) $mAhg^{-1}$. The ~75% reduction capacity decrease on cycling was similar to that previously[22] (and herein) observed for Ni_3N-lithium cells but note that a smaller drop in capacity is observed when only the oxidation (sodium-ion cell discharge) process is considered.

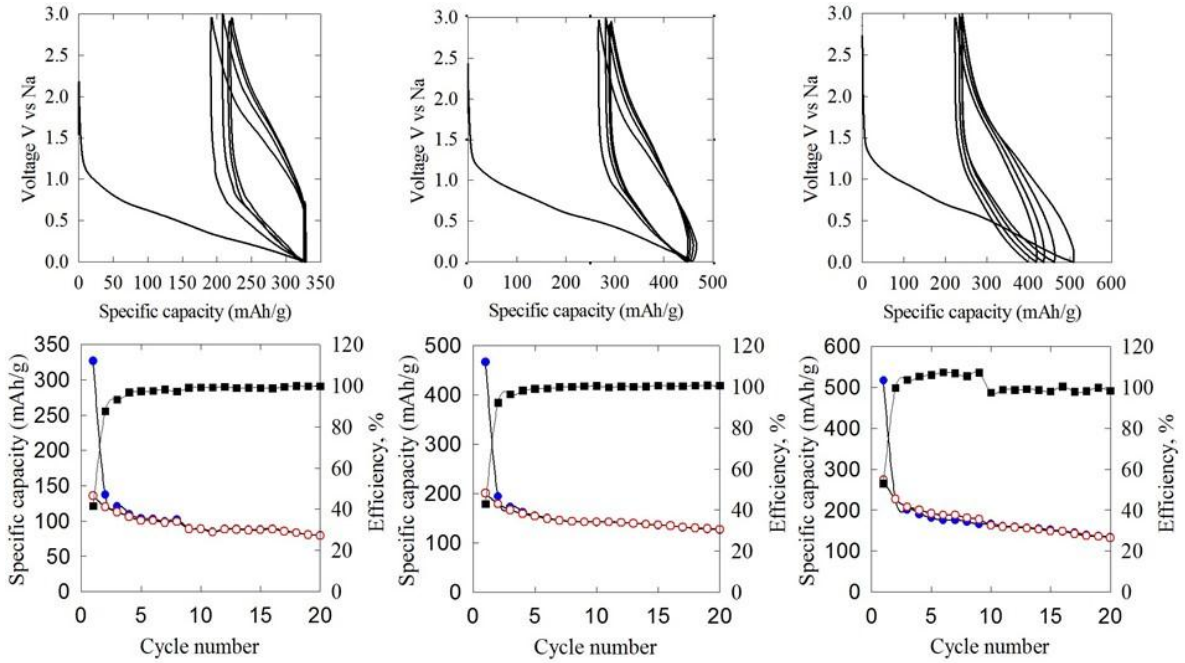

Fig. 5 Specific capacity during the first five reduction/oxidation cycles (top) and specific capacity versus cycle number profile (bottom) of Ni_3N-sodium half cells cycled between 1 mV and 3 V for 20 cycles at 1C (423 mAg^{-1}, left), 0.5C (211.5 mAg^{-1}, centre) and 0.1C (42.3 mAg^{-1}, right). In the specific capacity vs cycle number plots closed circles show specific reduction capacity, open circles show specific oxidation capacity and squares depict Coulombic efficiency.

The mechanism of charge storage by Ni_3N in sodium cells was investigated by recording X-ray diffraction data on an assembled Ni_3N composite electrode, electrochemically reducing it in a sodium half cell to 0.1 mV at a slow scan rate to maximise conversion, and re-recording the diffraction pattern (without air exposure) under identical conditions. In contrast to studies on Ni_3N thin films cycled vs Li where crystalline Ni was observed,[24] no new peaks were found suggesting that the reduction products were amorphous. Interestly, though, the Ni_3N peaks were only reduced in magnitude. This suggests that only the surfaces of the Ni3N crystallites is being utilised and hence that still smaller crystallites might result in the

availability of greater capacity. It is possible that the reducing capacity on cycling is due to gradual consumption of the Ni_3N active material, but note that after 20 cycles the specific oxidation capacity at 0.1C (134 $mAhg^{-1}$) is still 32% of the theoretical capacity of 423 $mAhg^{-1}$ for complete conversion to Ni metal and Na_3N, and that the intensity of the diffraction features is similar after 1 reduction or 20 reductions.

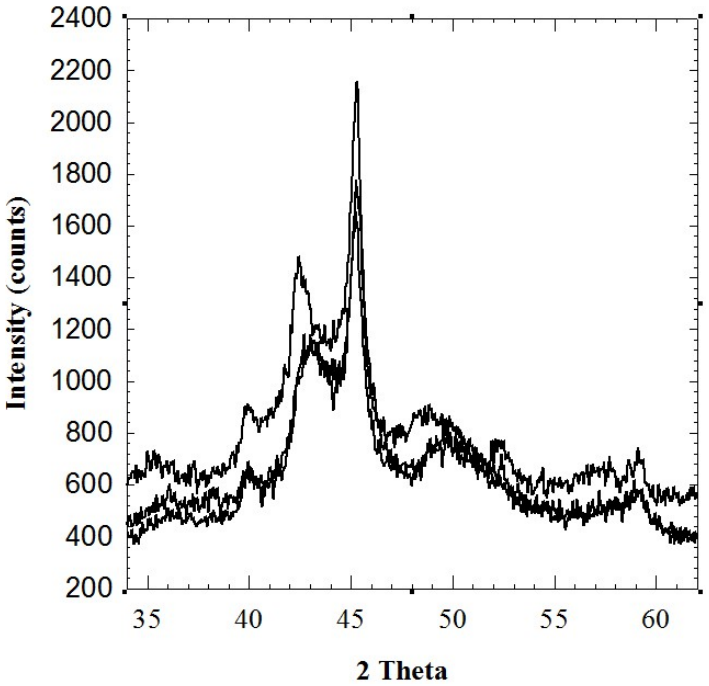

Fig. 6 Ex-situ PXD patterns of Ni_3N electrodes before any electrochemical cycling (top), and after reduction at a rate of 0.067C (28.2 mAg^{-1}) to 0.001 V (middle) and after reduction and oxidation at a rate of 0.5C (211.5 mAg^{-1}) for 20 cycles (bottom). PXD patterns were collected on identical samples before and after reduction with the same geometry and detector integration regions to ensure comparability.

The performance of Ni_3N as the active material for negative electrodes in sodium-ion cells is comparable with that of many of the best materials currently in the literature. The best capacity after 20 cycles (134 $mAhg^{-1}$) exceeds the capacity of carbon black, for which extended cycling studies were not reported, with charge and discharge over a similar potential range.[14] "Templated carbon"[15] and $NaTi_2(PO_4)_3$,[17] both deliver ~120 $mAhg^{-1}$ over this number of cycles, again with a similar potential range. "Hard carbon" has significantly higher capacity but was initially found to plate sodium during charging, making it unacceptable for use over multiple cycles due to the risk of dendrite formation.[12] A more recent study of hard carbon found it possible to utilise ~220 $mAhg^{-1}$ of this capacity reversibly (100+ cycles),[2] and a similar performance has been demonstrated in hollow carbon nanowire materials.[16] It is

likely that the already promising performance of Ni_3N might be further improved by reductions in particle size to bring it closer to this performance level, since the diffraction results show incomplete conversion in the present study.

Conclusions

Ni_3N shows good capacity and cycling characteristics on redox cycling vs sodium, and is a promising negative electrode material for sodium-ion batteries. This performance is competitive with the best nanoparticulate carbon materials.

References

1. J. M. Tarascon and M. Armand, *Nature*, 2001, **414**, 359.
2. S. Komaba, W. Murata, T. Ishikawa, N. Yabuuchi, T. Ozeki, T. Nakayama, A. Ogata, K. Gotoh and K. Fujiwara, *Adv. Funct. Mater.*, 2011, **21**, 3859.
3. B. L. Ellis and L. F. Nazar, *Curr. Opin. Solid State Mater. Sci.*, 2012, **16**, 168-177.
4. A. Mendiboure, C. Delmas and P. Hagenmuller, *J. Solid State Chem.*, 1985, **57**, 323.
5. A. Bhide and K. Hariharan, *Sol. St. Ionics*, 2011, **192**, 360.
6. P. Moreau, D. Guyomard, J. Gaubicher and F. Boucher, *Chem. Mater.*, 2010, **22**, 4126.
7. A. Caballero, L. Hernan, J. Morales, L. Sanchez, J. Santos Pena and M. A. G. Aranda, *J. Mater. Chem.*, 2002, **12**, 1142.
8. Y. Cao, L. Xiao, W. Wang, D. Choi, Z. Nie, J. Yu, L. V. Saraf, Z. Yang and J. Liu, *Adv. Mater.*, 2011, **23**, 3155.
9. H. Liu, H. Zhou, L. Chen, Z. Tang and W. Yang, *J. Power Sources*, 2011, **196**, 814.
10. S. Tepavcevic, H. Xiong, V. R. Stamenkovic, X. Zuo, M. Balasubramanian, V. B. Prakapenka, C. S. Johnson and T. Rajh, *ACS Nano*, 2011, **6**, 530.
11. Y. Lu, L. Wang, J. Cheng and J. B. Goodenough, *Chem. Commun.*, 2012, **48**, 6544.
12. P. Ge and M. Fouletier, *Sol. St. Ionics*, 1988, **28–30,**, 1172.
13. D. A. Stevens and J. R. Dahn, *J. Electrochem. Soc.*, 2000, **147**, 1271.
14. R. Alcántara, J. M. Jiménez-Mateos, P. Lavela and J. L. Tirado, *Electrochem. Commun.*, 2001, **3**, 639.
15. S. Wenzel, T. Hara, J. Janek and P. Adelhelm, *Energy Env. Sci.*, 2011, **4**, 3342.
16. Y. Cao, L. Xiao, M. L. Sushko, W. Wang, B. Schwenzer, J. Xiao, Z. Nie, L. V. Saraf, Z. Yang and J. Liu, *Nano Lett.*, 2012, **12**, 3783.
17. S. I. Park, I. Gocheva, S. Okada and J.-I. Yamaki, *J. Electrochem. Soc.*, 2011, **158**, A1067.
18. L. Wu, F. Pei, R. Mao, F. Wu, Y. Wu, J. Qian, Y. Cao, X. Ai and H. Yang, *Electrochim. Acta*, 2013, **87**, 41-45.
19. J. Qian, Y. Chen, L. Wu, Y. Cao, X. Ai and H. Yang, *Chem. Commun.*, 2012, **48**, 7070-7072.
20. L. Xiao, Y. Cao, J. Xiao, W. Wang, L. Kovarik, Z. Nie and J. Liu, *Chem. Commun.*, 2012, **48**, 3321-3323.
21. M. K. Datta, R. Epur, P. Saha, K. Kadakia, S. K. Park and P. N. Kumta, *J. Power Sources*, 2013, **225**, 316-322.
22. J. Cabana, L. Monconduit, D. Larcher and M. R. Palacín, *Adv. Mater.*, 2010, **22**, E170.
23. B. Das, M. V. Reddy, P. Malar, T. Osipowicz, G. V. Subba Rao and B. V. R. Chowdari, *Sol. St. Ionics*, 2009, **180**, 1061.
24. Y. Wang, Z.-W. Fu, X.-L. Yue and Q.-Z. Qin, *J. Electrochem. Soc.*, 2004, **151**, E162.
25. Q. Sun and Z.-W. Fu, *Electrochem. Sol-St. Lett.*, 2007, **10**, A189.
26. Q. Sun and Z.-W. Fu, *Electrochim. Acta*, 2008, **54**, 403.
27. F. Gillot, J. Oro-Sole and M. R. Palacin, *J. Mater. Chem.*, 2011, **21**, 9997.
28. S. Brunauer, P. H. Emmett and E. Teller, *J. Amer. Chem. Soc.*, 1938, **60**, 309.

29. N. S. Gajbhiye, Ningthoujam, R.S. and Weissmüller, J., *Phys. Status Solidi (a)*, 2002, **189**, 691.
30. H. M. Rietveld, *J. Appl. Cryst.*, 1969, **2**, 65.
31. D. V. Baxter, M. H. Chisholm, G. J. Gama, V. F. DiStasi, A. L. Hector and I. P. Parkin, *Chem. Mater.*, 1996, **8**, 1222.
32. K. Nakamoto, ed., *Infrared and Raman Spectra of Inorganic and Organic Compounds 3rd ed*, J. Wiley: New York, 1978.
33. C. Vidal-Abarca, P. Lavela, J. L. Tirado, A. V. Chadwick, M. Alfredsson and E. Kelder, *J. Power Sources*, 2012, **197**, 314.